Single, Dual and Tri-Band-Notched Ultrawideband (UWB) Antennas Using Capacitively Loaded Loop (CLL) Resonators

Chia-Ching Lin, *Associate Member, IEEE*, Peng Jin, *Member, IEEE*, and Richard W. Ziolkowski, *Fellow, IEEE*

***Abstract*—Two compact, printed, ultrawideband (UWB) monopole antennas with tri-band notched characteristics are reported. The notched filters are achieved by introducing printed, electrically small, capacitively-loaded loop (CLL) resonators. The directly driven elements consist of printed top-loaded CLL-based monopoles and 50 Ω microstrip feed lines. By adding three CLL elements close to the feed line, band-notch properties in the WiMAX (3.3–3.6GHz), lower WLAN (5.15–5.35GHz) and higher WLAN (5.725–5.825GHz) bands are achieved. Each antenna system is contained on a $27 \times 34\ \mathrm{mm}^2$ sheet of Rogers Duroid 5880 substrate. One is designed with three additional CLL elements; the other is achieved with only two. Comparisons between the simulation and measurement results show that these UWB antennas have broadband matched impedance values and stable radiation patterns for all radiating frequencies.**

***Index Terms*—Antenna efficiency, antenna pattern, antennas, metamaterials, ultrawideband (UWB).**

I. Introduction

ULTRAWIDEBAND (UWB) communication systems have become an attractive wireless topic since the Federal Communication Commission (FCC) first approved in 2002 the rules for the utilization of the 3.1–10.6 GHz unlicensed band for commercial UWB communications [1]. The high demands on such communication systems have stimulated research into many UWB antenna designs. Nonetheless, antenna designs for UWB applications face many challenges including their impedance matching, radiation stability, compact size, low manufacturing cost and electromagnetic interference (EMI) problems. The EMI problems are quite serious for UWB systems since there are several other existing narrowband services which occupy frequency bands within the designated UWB bandwidth. These include world interoperability for microwave access (WiMAX) service from 3.3 to 3.6 GHz; wireless local area network (WLAN) services such as IEEE 802.11a in the USA (5.15 to 5.35 GHz, 5.725 to 5.825 GHz) and HIPERLAN/2 in Europe (5.15 to 5.35 GHz, 5.47 to 5.725 GHz). To mitigate any interference with these coexisting systems, it is necessary to introduce a UWB antenna that has intrinsic filtering properties at their service frequencies. To minimize the footprint of the antenna system, the signal processing requirements, and the cost, it is highly desirable for those filters to be intrinsically handled rather than through any additional external band-stop filter devices.

There are several methods with which one can achieve a band-notched UWB antenna. The most popular approach is to embed different shaped slots in the radiating element or in its ground plane. Examples include U-shaped, H-shaped or C-shaped slots [2]–[6]. However, most UWB antennas have been designed with only one or two notched-frequency bands. On the other hand, the complimentary split ring resonator (CSRR) structure, for instance, was proposed recently to reject more than one of the unwanted frequency bands [7]–[9]. Although those designs are low profile, achieve stable radiation patterns, and have constant gain, the lower WLAN band (5.15–5.35 GHz) was not rejected successfully.

Two tri-band-notched UWB antennas are proposed in this paper. One design utilizes three electrically small resonators, each being realized as a capacitively-loaded loop (CLL). The CLL element was introduced originally to achieve a mu-negative metamaterial that acts as an artificial magnetic conductor for low profile antenna applications [10]. Each CLL element has a high-Q characteristic and a compact size, making it a very suitable candidate for a band-stop filter function. Like the split ring resonator (SRR) element [11], the CLL element is self-resonant and has a resonance frequency that is determined primarily by its loop inductance and the capacitances resulting from the cuts which open the loop. In contrast, the CLL element has a much simpler, more compact design. It will be demonstrated that by placing one, two or three CLL elements near the feedline and tuning their sizes, one can control the band-notched frequencies of the radiator, while minimizing their space requirements, to achieve single, dual, and tri-band notched-filter UWB antennas. The approach is analogous to the filter methods that introduce various types of metamaterial unit cell elements into transmission lines [12]. A second design employs a CLL-based slot element in the top-loaded monopole element and two CLL elements located along the feedline. It overcomes the tuning

Manuscript received March 17, 2011; revised June 08, 2011; accepted July 15, 2011. Date of publication September 15, 2011; date of current version January 05, 2012 This work was supported in part by DARPA Contract HR0011-05-C-0068 and in part by ONR Contract H940030920902.

C.-C. Lin was with the Department of Electrical and Computer Engineering, University of Arizona, Tucson, AZ 85721-0104 USA. He is now with Ruckus Wireless, Sunnyvale, CA 94085 USA.

P. Jin was with the Department of Electrical and Computer Engineering, University of Arizona, Tucson, AZ 85721-0104 USA. He is now with Broadcom Corporation, Irvine, CA 92617-3038 USA.

R. W. Ziolkowski is with the Department of Electrical and Computer Engineering, University of Arizona, Tucson, AZ 85721-0104 USA (e-mail: ziolkowski@email.arizona.edu).

Color versions of one or more of the figures in this paper are available online at http://ieeexplore.ieee.org.

Digital Object Identifier 10.1109/TAP.2011.2167947

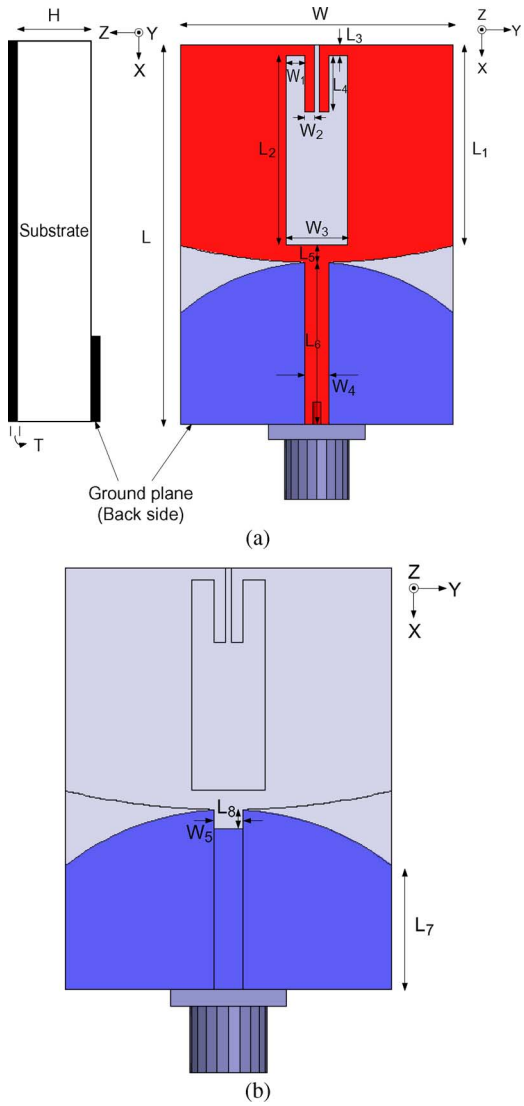

Fig. 1. Geometry of the baseline UWB antenna. (a) top view; (b) bottom view. All dimensions are in mm: $W = 27.0$, $W_1 = 1.8$, $W_2 = 1.0$, $W_3 = 6.0$, $W_4 = 2.4$, $W_5 = 2.4$, $L = 34.0$, $L_1 = 18.0$, $L_2 = 16.9$, $L_3 = 1.0$, $L_4 = 5.0$, $L_5 = 1.6$, $L_6 = 14.5$, $L_7 = 10.0$, and $L_8 = 1.5$.

sensitivities associated with the first design. Comparisons between the ANSOFT finite element method (FEM) based high frequency structure simulation (HFSS, v. 12.1) results and experiments for both designs show very good agreement. Initial results from these investigations were reported in [13].

II. UWB Antennas With and Without Band-Notched Filters

A. Baseline UWB Design

Fig. 1(a) and 1(b) show the top and bottom views of the baseline design. It is a top-loaded CLL-based UWB antenna that is implemented with Rogers Duroid 5880 board material. The latter has a relative permittivity $\varepsilon_r = 2.2$, loss tangent $\tan\delta = 0.0009$, 0.5 oz electrodeposited copper (17 μm thickness) and 31 mil thickness. Its overall size is $27\,(\mathrm{W}) \times 34\,(\mathrm{L}) \times 0.787\,(\mathrm{H})\mathrm{mm}^3$; it is fed by a microstrip line ($W_4 = 2.4$ mm) to achieve a 50 Ω input impedance when connected by an SMA

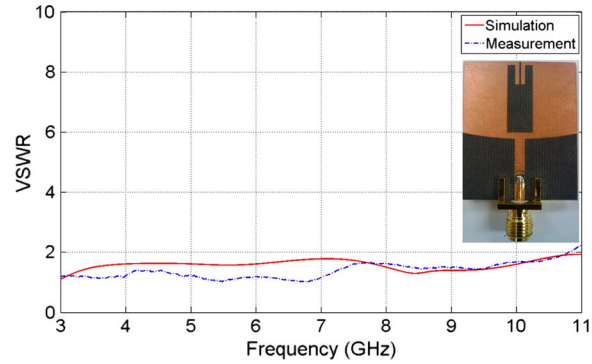

Fig. 2. Comparisons of the measured and simulated VSWR values for the baseline UWB antenna shown in Fig. 1.

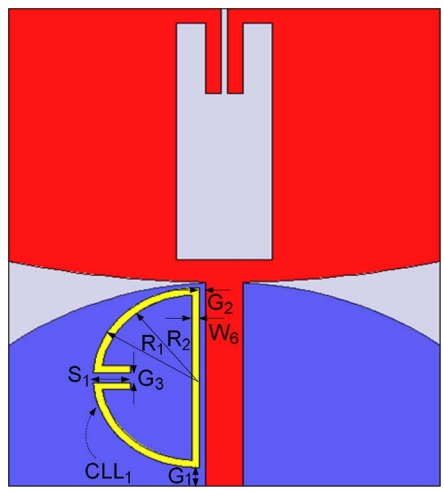

Fig. 3. Geometry of the single band-notched UWB antenna. All dimensions are in mm: $R1 = 6.4$ mm, $R2 = 5.9$ mm, $S1 = 2.3$ mm, $W6 = 0.5$ mm, $G1 = 1.3$ mm, $G2 = 0.35$ mm, and $G3 = 0.5$ mm.

connector to the source. The SMA connector is included in the HFSS model. The radiating portion of the antenna associated with the microstrip feed line is on one side (front) of the board; the conducting ground plane is on the other (back) side. Both the radiating monopole and the ground plane have curved shapes to help tailor the input impedance to a 50 Ω source, to increase the radiation efficiency and to help produce smooth transitions from one resonant mode to another. This characteristic ensures a good impedance match (i.e., VSWR ≤ 2) over the entire UWB frequency range, 3.1–10.6 GHz. The copper thickness and realistic values of its conductivity were included. The final optimization parameters and the measured and simulated VSWR values of the proposed UWB antenna are shown in Fig. 1 and Fig. 2, respectively. It is below 2 not only over the entire UWB band, but also at even higher frequencies.

B. Single Band-Notched UWB Antenna Design

In order to reduce the EMI with the WiMAX band, a band-notched function covering the interval 3.3–3.6 GHz is desired. The proposed single-notched UWB antenna is illustrated in Fig. 3. Notice that the gap region of the CLL_1 element has an augmented design to enhance its capacitance. By placing the CLL_1 element close to the feed line, this resonator is strongly coupled to it. It captures and stores all of the input energy at

TABLE I
COMPARISONS BETWEEN SIMULATIONS AND THEORETICAL PREDICTIONS OF THE BAND-NOTCHED FREQUENCY

L_{CLL} (mm)	Simulated frequency (GHz)	Theoretical frequency (GHz)
29	3.693	3.927
30	3.538	3.796
31	3.438	3.674
32	3.342	3.559

its resonance frequency and thus creates a single band-notched frequency filter. Note that with this design, there is no need to change the dimensions of the original UWB antenna. Rather, one simply needs to tune the resonance of the CLL_1 element by adjusting its dimensions to achieve the desired band-notched function. Moreover, this electrically small resonator has a minimal impact on other frequencies.

A parametric study of the CLL_1 element provides a necessary understanding of the interaction between the main radiator and the CLL_1 element. The band-notched frequency is given approximately by the expression

$$f_{notch} = \frac{c}{2L_{CLL} \cdot \sqrt{\varepsilon_{eff}}} \tag{1}$$

where L_{CLL} is the total length of the CLL_1 element, ε_{eff} is the effective dielectric constant, and c is the speed of the light. Given a desired resonance frequency, one can use (1) to define the initial total length of the CLL_1 element for an initial design. One can then use numerical simulations to adjust the dimensions of the CLL_1 element to obtain the final design. Table I shows a comparison between the simulated and theoretical predictions of the resonance frequency corresponding to different total lengths of the CLL_1 element. Note that the ability to further tune the CLL element by modifying its gap region is not only advantageous for achieving a specific band-notched function, but it also allows one to shrink the overall size of the CLL element. This provides one with the ability to add extra parasitic elements in a limited space and, hence, leads to a smaller-sized antenna without a loss in the desired functionality.

The HFSS-predicted VSWR values for the single-notched UWB antenna are shown in Figs. 4 and 5, respectively, for different lengths and sizes of the gap in the CLL element. Clearly, one can see that the length of the CLL_1 element and the size of its gap play critical roles in defining the band-notched frequency. For instance, the band-notched frequency decreases from 3.927 to 3.559 GHz as the length L_{CLL} increases from 29.0 to 32.0 mm. Similarly, because the capacitance decreases as the CLL gap size, G_3, increases, the band-notched frequency increases from 3.342 to 3.703 GHz as G_3 is varied from 0.5 mm to 2.0 mm. Note, however, that differences between the theoretical and simulated results in Table I also occur because of the coupling between the feedline and the CLL element. When the CLL_1 element is close to the feed line, the increased coupling produces extra capacitance, which then leads to a slightly lower band-notch frequency.

A comparison of the VSWR values for several gap sizes between the CLL_1 element and the feed line, G_2, is given in Fig. 6. One finds that as the CLL_1 element is moved closer to the feed line, a significant increase in the coverage of the band-notched frequency response occurs. For instance, the coverage of the band-notched frequency increases from 0.216 GHz to 1.108 GHz as G_2 decreases from 0.45 mm to 0.15 mm. Consequently, the location of the CLL_1 element also provides a means to adjust the coverage of the band-notched filter. These results further illustrate that when G_2 changes, there is only a small effect on the band-notch frequency, e.g., the shift is only 0.1 GHz in Fig. 6. We note that having control of the coverage of the band-notch filter is very important to achieving the desired, practical performance characteristics of a band-notched UWB antenna.

The final dimensions of the CLL_1 element for the single band-notched frequency design, as shown in Fig. 3. The

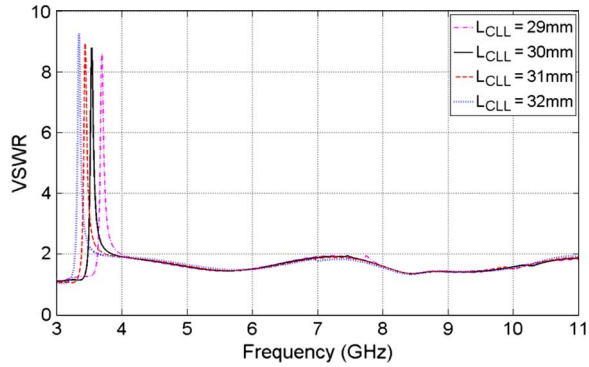

Fig. 4. HFSS-predicted VSWR characteristics for various total lengths (L_{CLL}) of the CLL element. The gap size (G_3) is fixed at 0.5 mm.

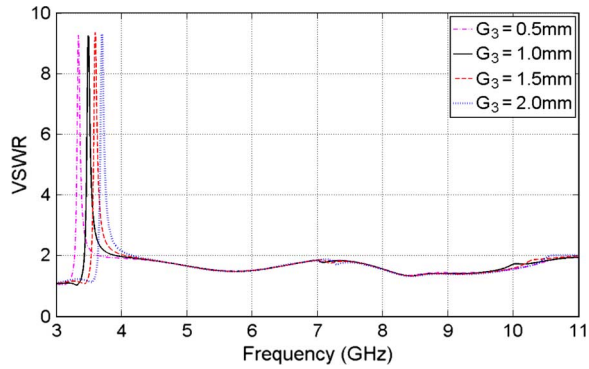

Fig. 5. HFSS-predicted VSWR characteristics for various CLL element gap sizes, G_3. The total length (L_{CLL}) of the CLL element is fixed at 32.0 mm.

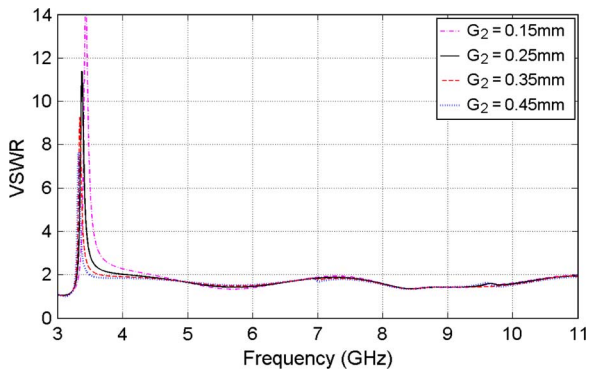

Fig. 6. HFSS-predicted VSWR values for various gap sizes (G_2) between the CLL element and the feedline. The total length (L_{CLL}) of the CLL element and its gap size (G_3) are fixed at 32.0 mm and 0.5 mm, respectively.

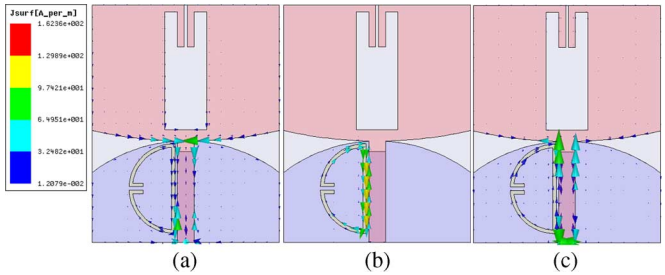

Fig. 7. HFSS-predicted surface current distributions at different frequencies. (a) 3 GHz, (b) 3.342 GHz, and (c) 10.0 GHz.

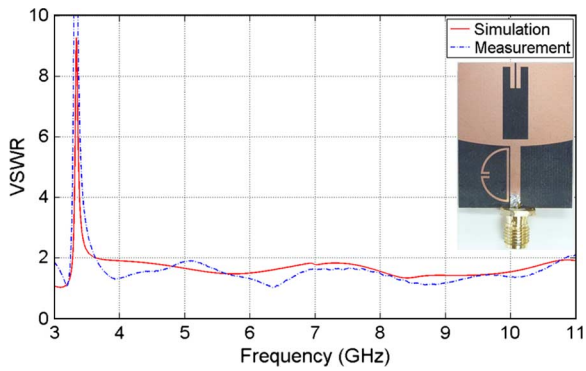

Fig. 8. Measured and HFSS-predicted VSWR values for the single band-notched UWB antenna.

HFSS-predicted current distributions at 3.0, 3.342 and 10.0 GHz are shown in Fig. 7. The currents flow mainly on the CLL_1 element at the notch frequency 3.342 GHz, while the currents on the radiating elements (the feedline and the monopole) at that frequency are very small. In contrast, the currents on the feedline and the monopole are large and negligible on the CLL_1 element away from the frequency band of the effective notched-filter.

The measured and simulated VSWR values versus frequency of the single band-notched UWB antenna are compared in Fig. 8. The measured bandwidth of the band-notched is from 3.25 to 3.62 GHz. As expected, the desired band-notched frequency is introduced by the CLL_1 element. Additionally, when compared to the original UWB antenna, the single band-notched UWB antenna successfully blocks the WiMAX band (3.3–3.6 GHz) and still maintains good impedance matching at the rest of the UWB band. The HFSS-predicted overall efficiency and maximum realized gain values are shown in Fig. 9 as a function of the frequency. As designed, significant drop of these values is observed within the rejection band.

C. Dual Band-Notched UWB Antenna Design

In addition to the WiMAX services from 3.3–3.6 GHz, the lower WLAN (5.15–5.35 GHz) band may also cause interference within the UWB band. To avoid EMI in this band, the dual band-notched UWB antenna and the optimized design parameters for the CLL_2 element shown in Fig. 10 was investigated. It is achieved simply by adding an additional CLL element near the feed line; i.e., the CLL_2 element is introduced on the other side of the feed line. To design a notch-band filter for the lower

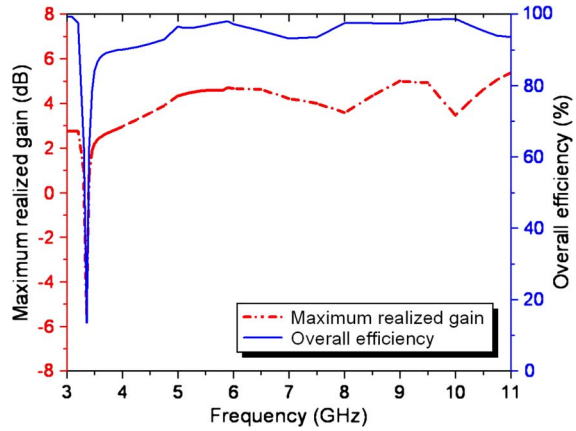

Fig. 9. The HFSS-predicted overall efficiency and maximum realized gain for the single band-notched UWB antenna.

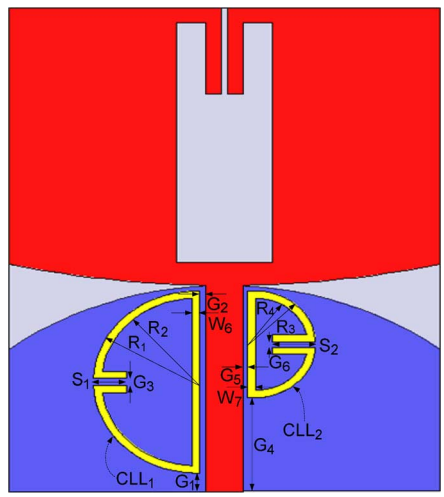

Fig. 10. Geometry the dual band-notched UWB antenna. All dimensions are in mm: $\mathrm{R}_3 = 3.75, \mathrm{R}_4 = 3.25, \mathrm{S}_2 = 2.69, \mathrm{W}_7 = 0.5, \mathrm{G}_4 = 6.6, \mathrm{G}_5 = 0.25$, and $\mathrm{G}_6 = 0.4$.

WLAN frequency set, one can still use (1) as the initial design to predict the approximate length of the CLL_2 element. Even though the CLL_2 element is added near the feed line, it was found (rather attractively) that the dimensions of the main radiator and CLL_1 element remain the same. Therefore, each CLL element is acting independently and, consequently, one obtains two band-stop filters at the different, desired frequencies.

The measured and simulated VSWR values versus frequency for the dual band-notched UWB antenna with two CLL elements (one on each side of the feedline) are compared in Fig. 11. Good agreement is observed. The measured dual band-notched frequencies cover 3.23–3.70 GHz and 5.09–5.58 GHz. The HFSS-predicted overall efficiency and maximum realized gain values versus frequency are shown in Fig. 12. They show the anticipated dramatic drop in these values at both band-notched frequency bands.

D. Tri-Band Notched UWB Antenna Design

Besides the WiMAX and lower WLAN bands, the higher WLAN band also operates within the UWB band. Again, to re-

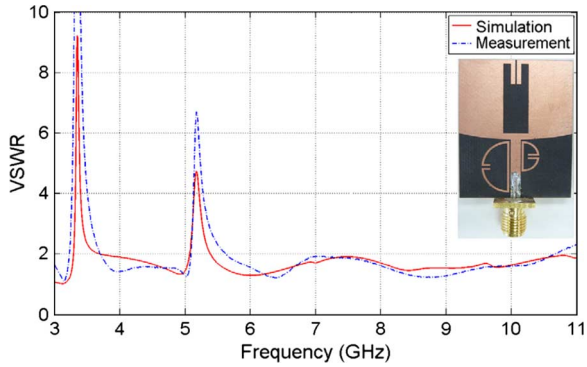

Fig. 11. Comparison of the measured and simulated VSWR values of the dual band-notched UWB antenna.

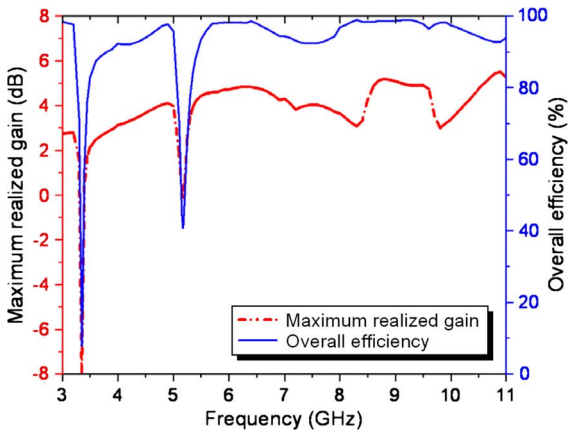

Fig. 12. The HFSS-predicted overall efficiency and maximum realized gain for the dual band-notched UWB antenna.

duce the potential EMI effects, a tri-band notched design was obtained. As with the single and dual band cases, the tri-band design begins with (1) to obtain the approximate length of the additional CLL element. However, the available area near the feed line limits where one can put a third CLL element. Nevertheless, as mentioned above, the benefit of the CLL element is its flexible tuning ability, i.e., the size of the gap region in the CLL element provides an extra degree of freedom to obtain the band-notched frequency within a specific area. Therefore, we simply shorten the total length of the CLL_2 element and decrease the gap size simultaneously to not only maintain the desired band-notched frequency, but also provide the extra area to add the additional CLL_3 element to realize the third band-notched frequency filter. Additionally, since the higher frequency WLAN band is narrower than the lower one, the gap between the CLL_3 element and the feed line should also increase. Again, the size of the main radiator and the ground plane size remain the same. Moreover, the dimension of the CLL_1 element also remains the same. Thus, the only difference between the dual and tri band-notched designs is to change the dimensions of the CLL_2 element in order to add the CLL_3 element. The proposed tri-band-notched UWB antenna and the correspondingly optimized parameters are shown in Fig. 13.

Good agreement between the HFSS-predicted and the measured VSWR values versus frequency is shown in Fig. 14 for the

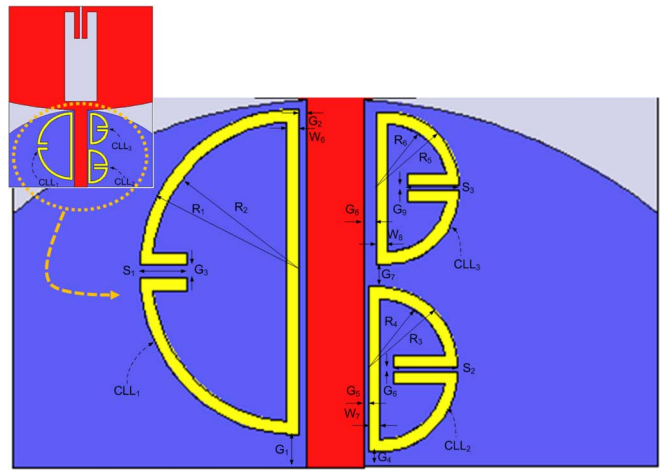

Fig. 13. The tri-band notched UWB antenna. (a) Geometry, and (b) design dimensions. All dimensions are in mm: $\mathrm{R}_3 = 3.25$, $\mathrm{R}_4 = 2.75$, $\mathrm{R}_5 = 3$, $\mathrm{R}_6 = 2.5$, $\mathrm{S}_2 = 2.7$, $\mathrm{S}_3 = 2.2$, $\mathrm{W}_7 = 0.5$, $\mathrm{W}_8 = 0.5$, $\mathrm{G}_4 = 0.6$, $\mathrm{G}_5 = 0.18$, $\mathrm{G}_6 = 0.15$, $\mathrm{G}_7 = 0.9$, $\mathrm{G}_8 = 0.5$, $\mathrm{G}_9 = 0.15$.

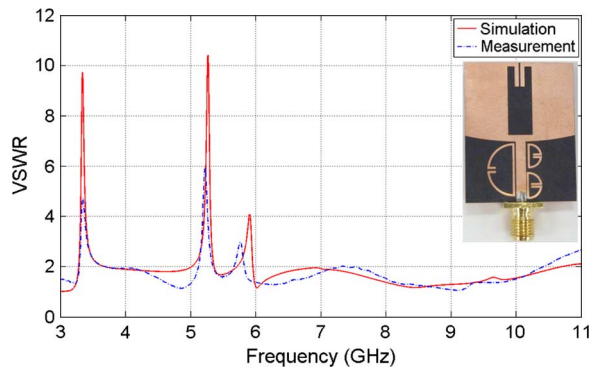

Fig. 14. Comparison of the measured and simulated VSWR values of the tri-band notched UWB antenna.

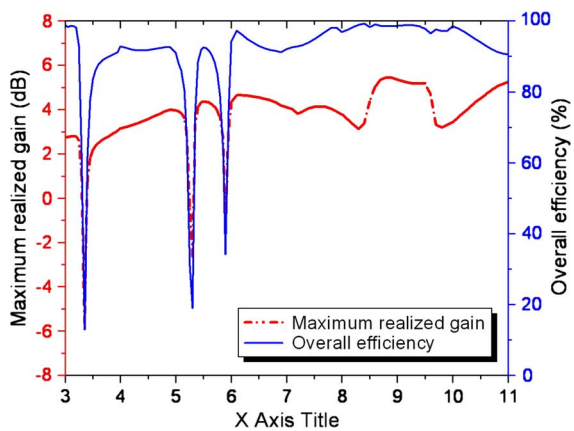

Fig. 15. The HFSS-predicted overall efficiency and maximum realized gain for the tri-band notched UWB antenna.

tri-band notched UWB antenna. The measured tri-band notches cover the bands: 3.29–3.67 GHz, 5.12–5.35 GHz and 5.67–5.83 GHz. As shown in Fig. 15, the antenna gain and radiation efficiency significantly decrease over these three band-notched frequency sets. The HFSS-predicted current distributions shown in Fig. 16 demonstrate that the currents flow around each CLL

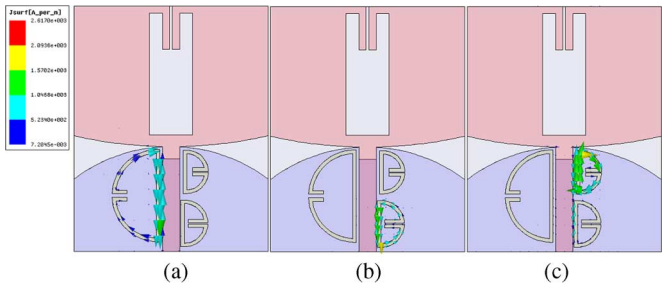

Fig. 16. HFSS-predicted current distributions at each band-notched frequency (a) 3.342 GHz (b) 5.279 GHz (c) 5.821 GHz.

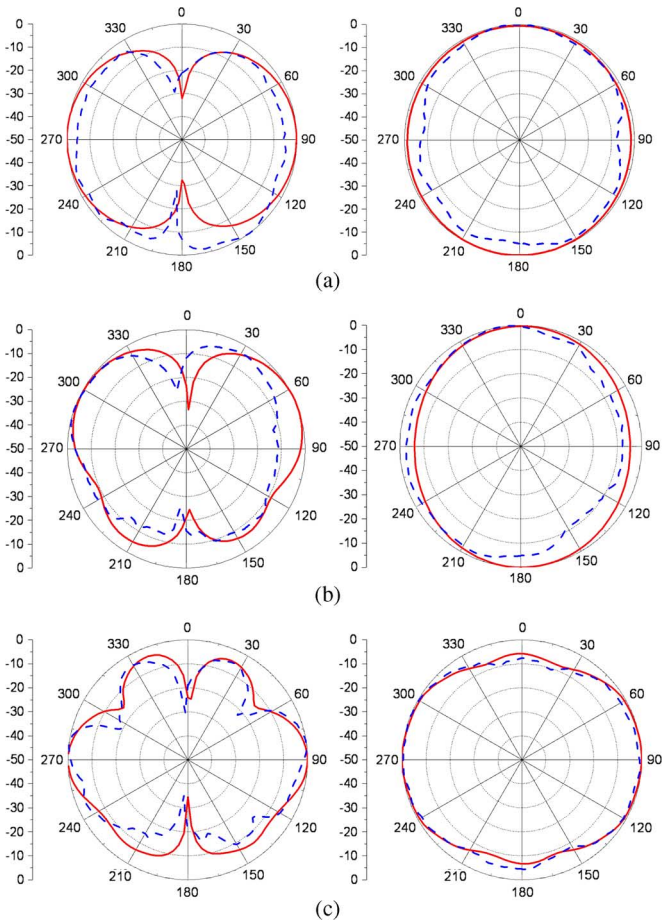

Fig. 17. The comparison between HFSS-predicted and measured radiation patterns (dB), E-Plane (left) and H-Plane (right), for the tri-band notched UWB antenna. (a) 3.1 GHz, (b) 5.5 GHz, (c) 10.6 GHz. Solid line: simulation; dashed line: measurement.

element only at the corresponding band-notch frequency. Additionally, one observes a small coupling between the CLL_2 and CLL_3 elements. Since the frequencies of the lower and higher WLAN bands are very close, less coupling would be desirable. One way to reduce this coupling is to increase the distance between the CLL_2 and CLL_3 elements. One could, for example, shorten the total length of each CLL element and decrease the gap size in order to have a much smaller sized CLL element and then increase the distance between the CLL_2 and CLL_3 elements. Unfortunately, this simple approach requires a much narrower gap in both the CLL_2 and CLL_3 elements; it leads to difficulties due to limitations of the fabrication techniques.

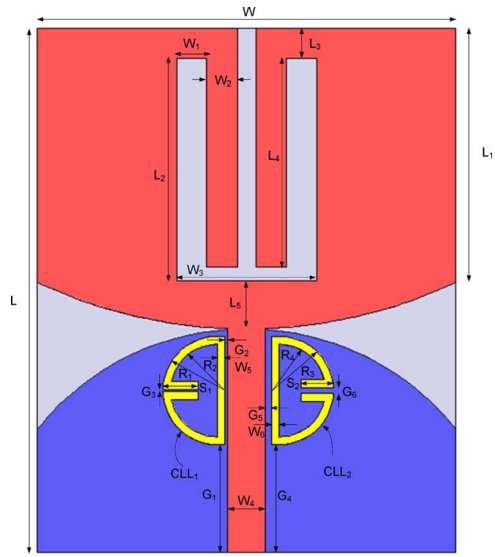

Fig. 18. Geometry of the tri-band notched UWB antenna with one slot CLL-based element in the top-loaded monopole and two CLL elements near its feedline. All dimensions are in mm: $\mathrm{W} = 27.0, \mathrm{W}_1 = 1.9, \mathrm{W}_2 = 2.0, \mathrm{W}_3 = 9.0, \mathrm{W}_4 = 2.4, \mathrm{W}_5 = \mathrm{W}_6 = 0.5, \mathrm{L} = 34.0, \mathrm{L}_1 = 16.5, \mathrm{L}_2 = 14.4, \mathrm{L}_3 = 2.0, \mathrm{L}_4 = 13.5, \mathrm{L}_5 = 3.1, \mathrm{R}_1 = 3.5, \mathrm{R}_2 = 3.0, \mathrm{R}_3 = 3.5, \mathrm{R}_4 = 3.0, \mathrm{S}_1 = 2.3, \mathrm{S}_2 = 2.09, \mathrm{G}_1 = 7.0, \mathrm{G}_2 = 0.2, \mathrm{G}_3 = 0.16, \mathrm{G}_4 = 7.0, \mathrm{G}_5 = 0.4$, and $\mathrm{G}_6 = 0.4$.

The HFSS-predicted and measured far-field radiation patterns for the proposed tri-band notched UWB antenna at 3.1, 5.5 and 10.6 GHz are shown in Fig. 17. Note that if the radiating element is assumed to be printed on the xy-plane, its radiation pattern is x-polarized because its monopole lies along the x-direction. Therefore, the E-plane is the xy-plane, while the H-plane is the yz-plane. The results shown in Fig. 17 demonstrate, as anticipated, that the H-plane patterns are omni-directional in all cases, while the E-plane patterns similarly exhibit the expected monopole-like behaviors. Distortions in the E-plane patterns begin to occur at higher frequencies because the radiating elements are no longer small relative to those wavelengths.

III. Alternative Tri-Band Notched UWB Antenna Design

Recall that while the coupling between the CLL_2 and CLL_3 elements in the tri-band notched design shown in Fig. 13 was small, the dimensions of those elements still had to be retuned to achieve the desired band-notched frequencies. As a consequence, the design becomes sensitive to the associated small gap regions needed to maintain their resonance frequencies while being smaller in size. Thus, it requires some effort to tune the entire system properly. To remove this sensitivity issue, we developed an alternative tri-band notched UWB antenna, shown in Fig. 18. It has one CLL-based slot element embedded in the top-loaded monopole and two additional CLL elements near the feedline. The idea is to tune the CLL-based slot element for the longer wavelength, lower frequency rejection band and then have the two, basically independent CLL elements near the feedline create the second and third band-notched filters. As the widths and lengths of this slot element are adjusted, its band-notch frequency can be tuned. This is illustrated with the single-notch version shown in Fig. 19. The measured and

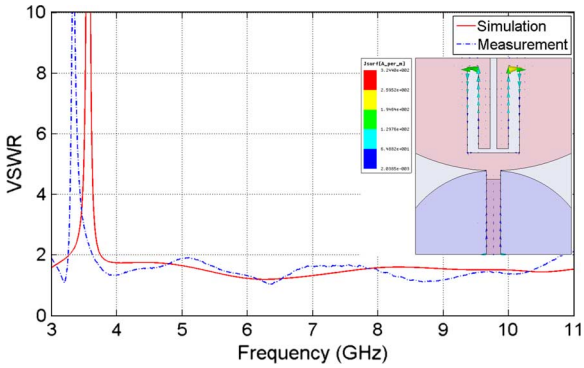

Fig. 19. Measured and simulated VSWR values for the single-notched UWB antenna. A CLL-based slot element is introduced into the top-loaded monopole to achieve the desired band-notched response at 3.35 GHz. The surface current distribution at this rejection frequency is localized near the slot element.

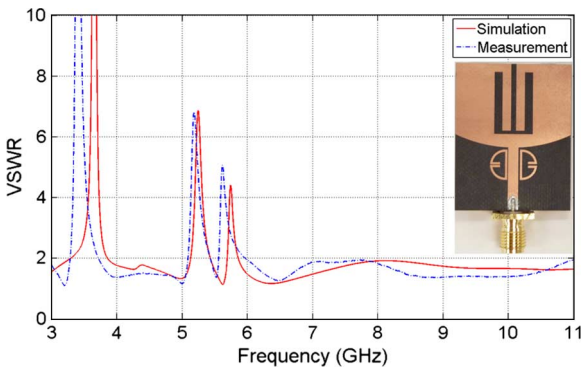

Fig. 20. Measured and simulated VSWR values versus frequency for the tri-band notched UWB antenna displayed in Fig. 18.

HFSS-predicted VSWR values are given along with the surface current distribution at 3.35 GHz, its band-notch frequency. Most of the currents are seen to flow around the gap region of the CLL-based slot element.

This embedded CLL-based design provides a more flexible tuning ability, particularly within the limited area close to the feed line. The two additional CLL elements are again located on opposite sides of the feedline. They were initially designed using (1). The final optimization parameters are shown in Fig. 18. Fig. 20 gives a performance comparison between the measured and simulated values of the VSWR versus frequency for the fabricated antenna. The measured tri-band notches cover 3.29.–3.72 GHz, 5.07–5.40 GHz and 5.62–5.93 GHz. As shown in Fig. 21, the antenna gain and radiation efficiency significantly decrease at these three band-notched frequencies and have high values away from them. We note that the measured upshifts in the lowest band shown in both Figs. 19 and 20 were consistent and found to be caused by fabrication errors. The fabricated slot widths were simply narrower than specified. We had emphasized the fabrication tolerances of the CLL elements with the vendor (Prototon Circuits, Tucson, AZ) anticipating that those of the larger slots would not be an issue. While this choice led to the very good agreement at the higher two-bands shown in Figs. 19 and 20, it clearly impacted the lower frequency band results.

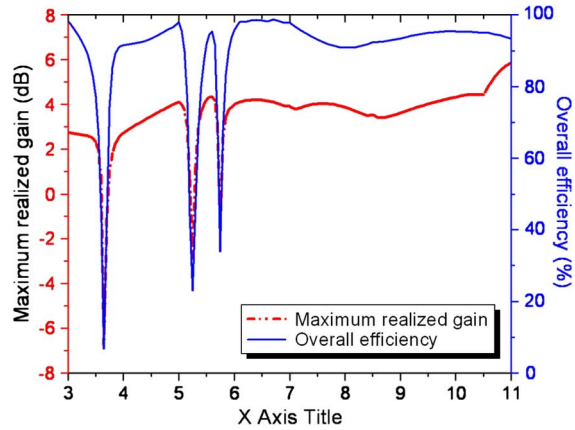

Fig. 21. The HFSS-predicted overall efficiency and maximum realized gain for the tri-band notched UWB antenna displayed in Fig. 18.

IV. Conclusions

Two CLL-based tri-band notched UWB antennas were introduced in this paper. They were obtained by using either three additional CLL elements or by embedding a CLL-based slot element into the top-loaded monopole and adding two CLL elements near the feed line. Single- and dual-notched band antennas were also considered to explain the performance characteristics of the tri-band designs. Parametric studies of all of these antennas provided guidelines on how to control not only the band-notched frequencies, but also the bandwidth of the rejected frequencies as well. The tri-band notched design with the three CLL elements had some sensitivities to achieve the band-notched characteristics for the closely adjacent frequencies associated with the lower and higher WLAN band that were overcome with the other design. By introducing the CLL-based slot element in the top-loaded monopole, the area limitations near feed line and the couplings introduced from the close proximity of two CLL elements were avoided. This design thus provided three independently tunable band-notch sets. The comparisons between the measured and simulated values for both tri-band notched UWB designs verified their predicted performance characteristics, including stable radiation patterns, high gain and radiation efficiencies, and broadband matched impedance values for all radiating frequencies

References

[1] Federal Communications Commission Revision of Part 15 of the Commission's Rules Regarding Ultra-Wideband Transmission System from 3.1 to 10.6 GHz Federal Communications Commission. Washington, DC, ET-Docket, 2002, pp. 98–153, FCC.

[2] W. S. Lee, D. Z. Kim, K. J. Kim, and J. W. Yu, "Wideband planar monopole antennas with dual band-notched characteristics," *IEEE Trans. Microw. Theory Tech.*, vol. 54, pp. 2800–2806, Jun. 2006.

[3] S. J. Hong, J. W. Shin, H. Park, and J. H. Choi, "Analysis of the band-stop techniques for ultrawideband antenna," *Microw. Opt. Technol. Lett.*, vol. 49, pp. 1058–1062, May 2007.

[4] X. L. Bao and M. J. Ammann, "Printed band-reject UWB antenna with H-shaped slot," in *Proc. IEEE IWAT Workshop*, Mar. 2007, pp. 319–322.

[5] Q. Chu and Y. Yang, "A compact ultrawideband antenna with 3.4/5.5 GHz dual band-notched characteristics," *IEEE Trans. Antennas Propag.*, vol. 56, pp. 3637–3644, Dec. 2008.

[6] H. Zhang, R. Zhou, Z. Wu, H. Xin, and R. W. Ziolkowski, "Designs of ultra wideband (UWB) printed elliptical monopole antennas with slots," *Microw. Opt. Technol. Lett.*, vol. 52, pp. 486–471, Feb. 2010.
[7] J. Kim, C. S. Cho, and J. W. Lee, "5.2 GHz notched ultra-wideband antenna using slot-type SRR," *Electron. Lett.*, vol. 42, pp. 315–316, Mar. 2006.
[8] J. Liu, S. Gong, Y. Xu, X. Zhang, C. Feng, and N. Qi, "Compact printed ultra-wideband monopole antenna with dual band-notched characteristics," *Electron. Lett.*, vol. 44, pp. 710–711, Jun. 2008.
[9] J. Ding, Z. Lin, and Z. Ying, "A compact ultra-wideband slot antenna with multiple notch frequency bands," *Microw. Opt. Technol. Lett.*, vol. 49, pp. 3056–3060, 2007.
[10] A. Erentok, P. Luljak, and R. W. Ziolkowski, "Antenna performance near a volumetric metamaterial realization of an artificial magnetic conductor," *IEEE Trans. Antennas and Propag,*, vol. 53, pp. 160–172, Jan. 2005.
[11] J. B. Pendry, A. J. Holden, D. J. Robbins, and W. J. Stewart, "Magnetism from conductors, and enhanced non-linear phenomena," *IEEE Trans. Microwave Theory Tech.*, vol. 47, pp. 2075–2084, Nov. 1999.
[12] R. Marqués, F. Martín, and M. Sorolla, *Metamaterials With Negative Parameters: Theory, Design and Microwave Applications*. Hoboken, NJ: Wiley, 2008.
[13] C.-C. Lin and R. W. Ziolkowski, "Tri-band notched ultra-wideband antenna using capacitively loaded loops," presented at the Int. Symp. on Antennas and Propagation, Toronto, Canada, Jul. 2010, paper 408.4.

Chia-Ching Lin (S'07–A'11) received the B.Sc. and M.Sc. degrees in electronic engineering from the National Taiwan University of Science and Technology (NTUST), in 1999 and 2003, respectively, and the ECE Ph.D. degree from the University of Arizona, Tucson, in 2010.

He is currently with Ruckus Wireless, Sunnyvale, CA. His research interests include electrically small antennas and metamaterial applications to antenna designs.

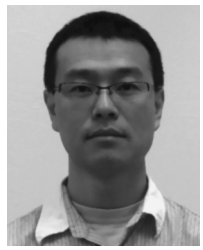

Peng Jin (S'05–M'10) received the EE B.Sc. degree from the University of Science and Technology of China, Heifei, in 1999, the EE M.Sc. degree from the North Dakota State University, Fargo, in 2004, and the ECE Ph.D. degree from the University of Arizona, Tucson, in 2010.

He is currently with the Signal Integrity Group, Broadcom Corporation, Irvine, CA. His research interests include electrically small antennas and metamaterial applications to antenna designs.

Richard W. Ziolkowski (M'87–SM'91–F'94) received his Sc.B. degree in physics, magna cum laude with honors, from Brown University (1974), his M.S. (1975) and Ph.D. (1980) degrees in physics from the University of Illinois at Urbana-Champaign. He was a member of the Engineering Research Division at the Lawrence Livermore National Laboratory from 1981 to 1990 and served as the leader of the Computational Electronics and Electromagnetics Thrust Area for the Engineering Directorate. He currently is serving as the Litton Industries John M. Leonis Distinguished Professor in the Department of Electrical and Computer Engineering at the University of Arizona. He holds a joint appointment with the College of Optical Sciences. He is an IEEE Fellow and an OSA Fellow. He was the President of the IEEE Antennas and Propagation Society in 2005. He continues to be very active in the IEEE, OSA, and APS professional societies. He has served on the International Advisory Boards and Technical Program Committees of several international conferences, including iWAT, ISAP, Metamaterials, and META. His research interests include the application of new physics and engineering ideas to linear and nonlinear problems dealing with the interaction of electromagnetic waves with complex media, metamaterials, and realistic structures.